

Purdue Physics REU Final Presentations & Abstracts

August 2, 2018

9:00 Anya Wolterman (Prof. Jung)
9:20 Whitney Weinschenk (Prof. Pushkar)
9:40 Urayoan Verges (Prof. Kais)
10:00 Rachel Taubman (Prof. Iyer-Biswas)

10:20 – 10:30 *break*

10:30 Eric Putney (Prof. Elliott)
10:50 Colin Riggert (Prof. Robicheaux)
10:10 Melissa Popeil (Prof. Huang)
10:30 Scott McKinley (Prof. Slipchenko)

11:50 - 1:20 *Lunch (on your own)*

1:20 Kevin Knox (Prof. Hung)
1:40 Caitlin Gish (Prof. Ritchie)
2:00 Leesa Brown (Prof. Lang)
2:20 William Braverman (Prof. Pyrak-Nolte)

2:40 *The end*

6:30 - *Farewell party/picnic at Sergei Savikhin's house for REU students, advisors, speakers & significant others*

Address: 2505 McShay Dr., West Lafayette
Phone: 765-413-5026 (cell)

Through-Plane Thermal Conductivity Measurements for the Phase II Upgrade of the CMS Pixel Detector

*Anya Wolterman*¹, *Andrew Wildridge*², *Abraham Kosky*², *Souvik Das*², *Andreas Jung*²

¹Macalester College, MN, ²Purdue University, IN

The Large Hadron Collider (LHC) at CERN has made important contributions to particle physics since it first started collecting meaningful data in 2010, such as the discovery of the Higgs boson in 2012. Beams of highly relativistic particles meet in various detectors around the LHC's 27-km circumference, where the collisions are so energetic that a significant portion of the beams' energy is converted into mass, thereby creating new particles not seen under normal conditions. In the Compact Muon Solenoid (CMS) Experiment, a general purpose detector at the LHC, scientists use these collisions to study the Standard Model, investigate candidates for dark matter, and search for extra dimensions. The LHC has been upgraded multiple times over the last several years to allow it to reach progressively higher beam energies and produce even more collisions. The next major upgrade—known as the High Luminosity LHC Upgrade and currently scheduled for 2023—will generate a higher particle flux than ever before and increase the luminosity to unprecedented levels. While this will increase the probability of observing more rare processes and exotic particles, it will also cause the silicon detectors in the CMS tracking system to experience more radiation than they are designed to handle. Thus, the innermost tracking layers of the CMS Pixel Detector will need to be made more radiation-resistant in light of this increased luminosity. 3D silicon detectors, in the form of pixels and strips, are promising candidates given their superior radiation hardness compared to conventional planar silicon detectors, and Purdue has taken a leading role in developing this technology. The new silicon sensors and their attached readout electronics will be mounted on a lightweight substrate composed of carbon fiber and carbon foam with tubes of saturated liquid CO₂ running through it to cool the system (see Figure 1). Our goal is to determine the thermal performance of the materials that will be used in these half-disk structures. Knowing their thermal properties will allow us to better simulate heat conduction in different direction and therefore better predict how they'll work in the detector itself.

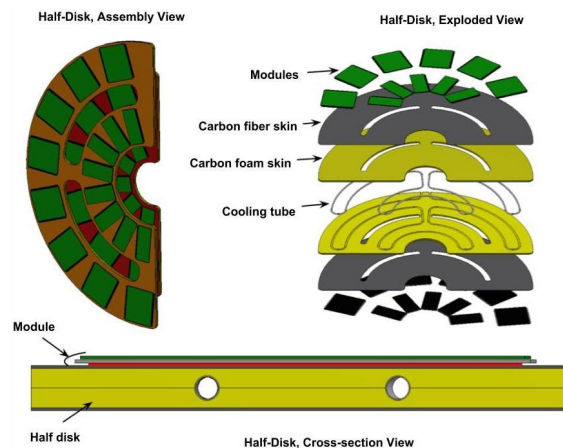


Figure 1

My objective was to determine the through-plane thermal conductivity of the various materials that will be used in the upgraded detector. This was done using an apparatus that features two cylindrical blocks of copper, one attached to a resistive heating element and the other to a Peltier cooler, each with a series of thermistors installed along their length on either side of a sample disk of a certain thickness. The materials tested include K13C2U, K13D2U, carbon weave, epoxy, and quartz (for calibration). The heater and cooler establish a temperature difference across the copper blocks and the sample, thereby generating a heat flux q through both materials according to Fourier's Law, $q = -k\nabla T$, where k is the thermal

conductivity of the material and ∇T is the temperature gradient—which we assume to be continuous and therefore equal to the difference in temperature across a distance. The average heat flux through the sample is calculated based on our determinations of the flux through each copper block—using Fourier’s Law since copper has a known thermal conductivity and the temperature gradient can be found from the thermistors’ positions and steady-state temperature readings. The temperature difference across the sample itself comes from extrapolating the linear regressions of the temperature versus position plots for the hot and cold flux meters. A linear fit to a plot of the temperature difference over the heat flux as a function of sample thickness (see Figure 2) would satisfy the equation $\Delta T/q = x/k + 2/h$, where h is the thermal conductance of the interface and k is the thermal conductivity of the sample. For materials with samples of at least three different thicknesses, our best estimate of k —one that excludes the interfaces between the copper and the sample—comes from the reciprocal of the slope of such a plot.

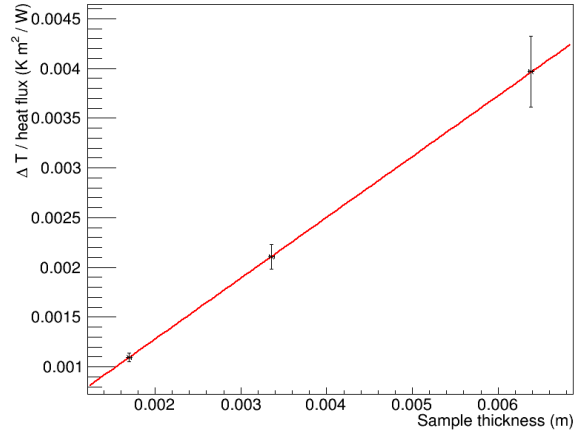


Figure 2

In addition to preparing and running the tests for each material then analyzing the results to produce an estimate of k , I was tasked with calibrating the thermistors in the through-plane apparatus. By submerging

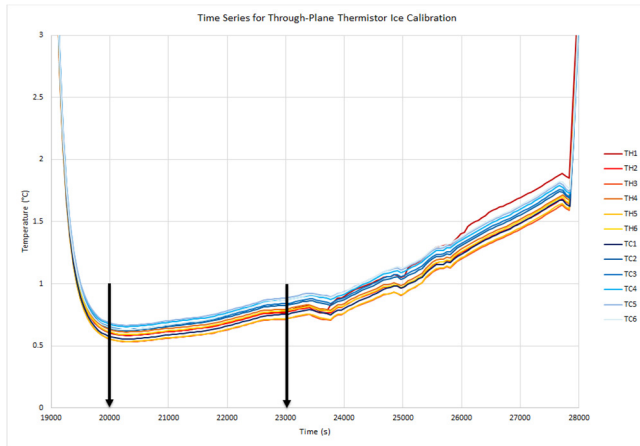


Figure 3

all of the thermistors in a tub of ice and water and collecting a plot of the temperature read by each thermistor over time (see Figure 3), I was able to determine the appropriate correction factors and uncertainties for each thermistor’s temperature reading. These values were then implemented in our calculations of the average heat flux and the temperature difference which in turn updated our estimates of k and resulted in a significant decrease in the uncertainty in those estimates.

I would like to thank Professor Jung and everyone in the Purdue Silicon Detector Laboratories working on this project for their guidance and assistance, and the Purdue Physics Department for providing me with resources and facilities to perform this research. I would also like to thank the NSF REU program for affording me this opportunity and NSF REU grant PHY-1460899 for supporting my work.

Water Oxidation Using Natural and Artificial Methods

Whitney Weinschenk¹, Scott Jensen², Alireza K. Ravari², Roman Ezhov², Yulia Pushkar²

¹DePauw University, IN, ²Purdue University, IN

In photosynthesis, Photosystem II (PSII), a photoactive metalloprotein complex, performs water oxidation, splitting water into molecular oxygen, protons, and electrons. A photon is absorbed by the chlorophyll on PSII which transfers the energy to the special pair in PSII, which is responsible for charge separation.¹ The special pair uses this energy to oxidize a tyrosine which sends an electron down the electron transport chain. The Mn₄Ca-cluster, or Oxygen Evolving Complex, replaces the electron in the tyrosine, which ultimately comes from water. After photo absorption has occurred four times, two water molecules are split and become one oxygen molecule (O₂) and four protons in solution (H⁺). This is studied because hydrogen is an alternative clean burning fuel and if the process of natural water oxidation can be understood, then it can be reproduced artificially and efficiently.

During the beamtime at the Advanced Photon Source at Argonne National Laboratory, we observed the oxidation states of the Mn atoms in the Oxygen Evolving Complex to better understand the S-states and how they differ. Each S-state represents a different oxidation state of the cluster. These observations were conducted by exciting the chlorophyll through the use of a 532nm laser. The S-states were studied because the transition from S₃ to S₀ remains poorly characterized.¹ There is an intermediate step between the two states that is only theorized, which was part of what we were trying to observe. However, more studies will need to be conducted to fully understand this transition.

Along with our observations of natural water oxidation, we are studying artificial photosynthesis using Ruthenium, a well-established catalyst for water oxidation. Water oxidation catalysts and artificial photosynthesis can be used to store solar energy by converting the sunlight and water into fuels, however, there are limitations. The rate observed for the water oxidation reaction is rather slow, the catalysts are somewhat unstable and costly, and we are currently unable to integrate essential components for complete reactivity in an effective way.² To aid in reducing these limitations, we are studying the oxygen evolution rates and lag phases of water oxidation catalysts after the addition of Cerium Ammonium Nitrate (CAN), which energizes the catalysts to create low-energy pathways from water to molecular oxygen and hydrogen.

My objective in this project was to generate oxygen evolution profiles for different concentrations of CAN with various water oxidation catalysts to determine which catalysts would best be suited for further study. To do this, I conducted oxygraphic studies using 0.1 mM catalysts in water and various concentrations of CAN in 1 M HNO₃. The oxygraph uses an electrode to determine the oxygen evolution of the samples by measuring the concentration of dissolved O₂. Through my experiments and analysis of the data I have determined that of the catalysts that were tested, Ru(bpy)(dcbpy) (bpy=2,2'-bipyridine, dcbpy=5,5-dicarboxy-2,2'-bipyridine) is the best candidate for further studies as it produces the highest oxygen evolution rate (Figure 1) and has no lag phase after the addition of CAN (Figure 2). The next step in this study will be to incorporate Ru-based water oxidation catalysts onto FTO (fluorine doped tin oxide) plates and test their catalytic abilities through electrochemistry.

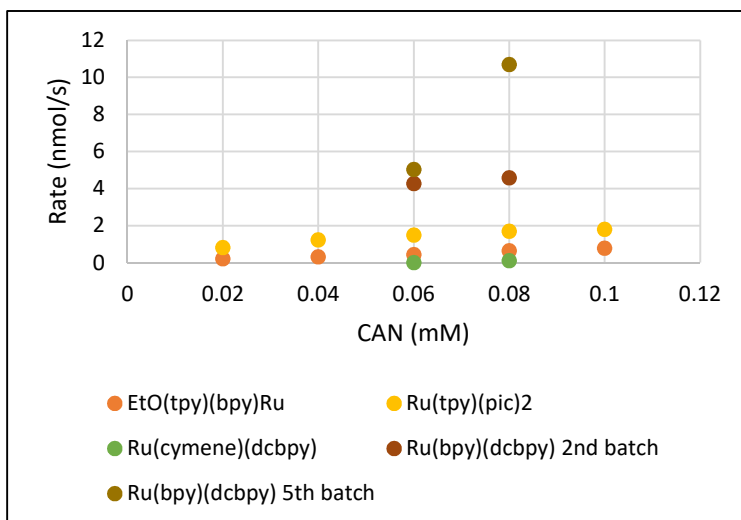


Figure 1. Rate of oxygen evolution in catalysts with various concentrations of Cerium Ammonium Nitrate (CAN). (bpy=2,2'-bipyridine, dcbpy= 5,5-dicarboxy-2,2'-bipyridine, tpy= 2,2':6'2''-terpyridine, pic=picolinate)

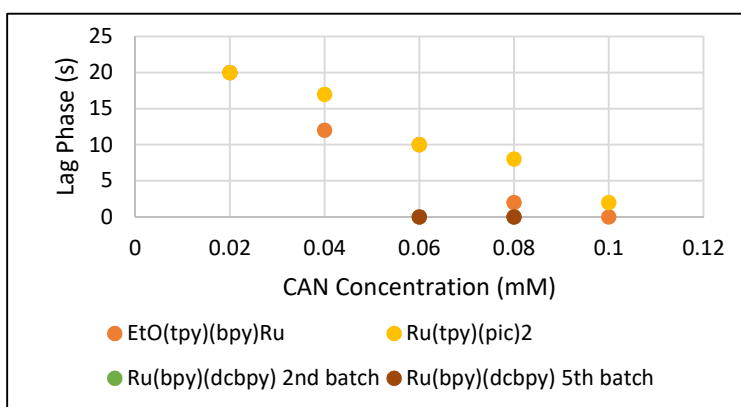


Figure 2. Lag phases of catalysts with various concentrations of Cerium Ammonium Nitrate (CAN). The second batch of Ru(bpy)(dcbpy) has no lag phase and the points are beneath the fifth batch points. Ru(cymene)(dcbpy) was excluded from this figure as the lag phases ranged from more than 3 minutes to more than 19 minutes and would have skewed the graph.

I am thankful for the opportunity to be a part of the REU program at Purdue University. I would like to thank Professor Yulia Pushkar, Scott Jensen, Alireza K. Ravari, and Dr. Roman Ezhov for their guidance during this experience. I would also like to thank NSF grant CHE-1350909 for supporting my work and for the use of the Advanced Photon Source, an Office of Science User Facility operated by the U.S. Department of Energy (DOE) Office of Science by Argonne National Laboratory, which was supported by the U.S. DOE under Contract No. DE-AC02-06CH11357.

¹Davis, et. al. *Rapid Evolution of the Photosystem II Electronic Structure during Water Splitting*. arXiv: 1506.08862 [physics.bio-ph] (2015).

²Lin, et. al. *Electrochemical Water Oxidation by a Catalyst-Modified Metal-Organic Framework Thin Film*. *ChemSusChem* **2016**, 9, 1-10.

Larger integer values, such as 25, 35, 49 gave resulting matrices of size 64×64 , the diagonal values of these matrices are displayed in fig. 2.

Sorted Energy Values for 6 Qubit Ising Model			
i Value	Diagonal a_{ii} element in the matrix for $N =$ 25	Diagonal a_{ii} element in the matrix for $N =$ 35	Diagonal a_{ii} element in the matrix for $N =$ 49
1	0	0	0
2	8	0	98
3	8	50	98
4	50	98	288
5	50	98	384
6	50	98	384
7	50	200	392
8	128	200	392
9	162	338	578
10	162	392	578
11	200	392	674
12	200	450	674
13	242	450	800
14	242	482	882
15	288	482	882
16	288	512	896
17	626	512	968
18	626	576	968
19	672	576	1058
20	672	578	1058
21	712	802	1096
22	712	802	1096
23	882	994	1152
24	882	1010	1248
25	930	1010	1248
26	930	1032	1250
27	960	1032	1250
28	960	1152	1410
29	960	1152	1410
30	960	1160	1538
31	968	1160	1538
32	968	1160	1544
33	1010	1160	1544
34	1010	1170	1632
35	1010	1170	1632
36	1010	1218	1650
37	1160	1218	1650
38	1160	1250	1698
39	1184	1250	1698
40	1202	1280	1736
41	1202	1280	1736
42	1650	1600	1826
43	1650	1600	1826
44	1736	1826	2120
45	1736	1826	2120
46	1920	2098	2336
47	1970	2120	2498
48	1970	2120	2498
49	2048	2130	2592
50	2592	2880	3426
51	2592	2880	3426
52	2610	2882	3456
53	2610	2882	3456
54	2696	2946	3464

55	2696	2946	3464
56	2850	3080	3570
57	2850	3080	3570
58	3490	3720	4210
59	3490	3720	4210
60	3506	3776	4322
61	3506	3776	4322
62	3592	3824	4360
63	3592	3824	4360
64	5024	5314	5888

Fig. 2. Table expressing the diagonal values of all the 64×64 matrices worked on in the project. These are $N = 25, N = 35$ and $N = 49$

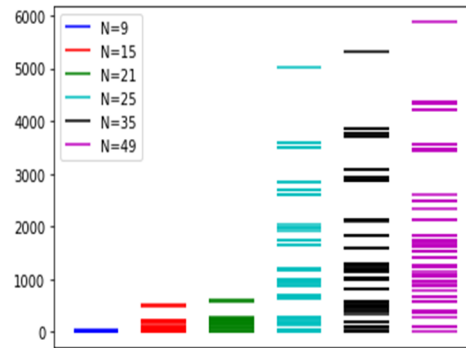


Fig. 3. Energy Levels for the Hamiltonians.

Some patterns can be seen in the data. Some energy levels are repeated between same-size energy levels, and they are all segmented into major clusters of energy levels. Even so, no mathematical relation has been found to transform one matrix to the other. Further research is necessary to give more conclusive evidence of a possible physical relation.

Acknowledgements: I would like to thank Prof. Sabre Kais for guiding me and granting me the opportunity of working with him during this Summer Internship program. Special thanks to the program coordinators for granting me the opportunity of taking part in this wonderful experience. This work was supported by NSF REU grant PHY-1460899.

¹ S. Jiang, K. A. Britt, T. S. Humble, S. Kais. Quantum Annealing for Prime Factorization. *arXiv preprint arXiv:1804.02733*. 2018

² R. Dridi, H. Alghassi. Prime factorization using quantum annealing and computational algebraic geometry. *arXiv preprint arXiv:1604.0579*. 2016

Stochastic Growth and Division of *Asticcacaulis Biprosthecum*

Rachel Taubman,

in the group of Prof. Srividya Iyer-Biswas

Purdue University, IN

Until recent years, observation of individual bacteria for extended periods of time was nearly impossible due to rapid exponential growth of the cell population, crowding fields of view. Thus obtaining quantitative results on the stochastic dynamics of a population of statistically identical cells has been a longstanding experimental challenge. This posed a significant barrier to studying probabilistic cell growth and division dynamics using a top-down, minimalist, physics approach. The novel SChemostat method developed by Professor Iyer-Biswas and her colleagues facilitates observation of dimorphic bacteria for multiple generations with unprecedented statistical precision. Use of this quantitative method has already yielded significant insights into scaling laws for the bacteria strain *Caulobacter crescentus*, revealing that an emergent condition-specific cellular unit of time governs all aspects of stochastic growth and division for *Caulobacter* (1). The question remains as to whether these results are universal across many other bacteria strains. If this were the case, it would suggest that many cellular processes could be described by simple timescales and that these timescales might be manipulated in order to control innumerable biological systems.

The goal of this research project was to gather population-level and single cell growth data for bacteria strain *Asticcacaulis biprosthecum*, which has a life cycle similar to that of *Caulobacter crescentus*, with motile and stalked phases. First, studies were done to determine the population growth rate of *Asticcacaulis* cells incubated at different temperatures in PYE media. These trials showed that *Asticcacaulis* population-level growth is exponential with doubling times roughly twice that of *Caulobacter*. A different *Asticcacaulis* growth method described by Larson and Pate (2) was attempted, but it resulted in cultures with more varied and lower optical densities. Potential effects on cell shape or durability resulting from the alternate growth method, as suggested in (2), have not yet been analyzed in single-cell experiments. Two single-cell *Asticcacaulis* experiments were conducted at 24°C. Preliminary analysis of single-cell data from 28°C suggests that *Asticcacaulis biprosthecum* does have an emergent condition-specific timescale which governs universal statistics of growth and division. Preliminary results from population data indicate that it may be possible to provide a unified multi-scale description, bridging the scales of single-cell and population growth dynamics (3).

Thank you to Professor Iyer-Biswas for her guidance, support, and lectures on stochastic processes, to all members of the Iyer-Biswas lab for explaining the single-cell experimental procedure and data analysis process, and to the National Science Foundation for funding through the REU grant PHY-1460899.

References

1. Iyer-Biswas S, Wright C, Jonathan H, Lo K, Stanislav Burov, Yihan Lin, Gavin E. Crooks, Sean Crosson, Aaron R. Dinner, Norbert F. Scherer (2014) Scaling laws for single cells. *Proceedings of the National Academy of Sciences* 11 (45) 15912-15917
2. Larson, R.J. & Pate, J.L. *Arch. Microbiol.* (1975) 106: 147. <https://doi.org/10.1007/BF00446517>
3. Jafarpour F, Wright C, Gudjonson H, Riebling J, Dawson E, Lo K, Fiebig A, Crosson S, Dinner A, and Iyer-Biswas S (2018) Bridging the Timescales of Single-Cell and Population Dynamics, *Phys. Rev. X* 8, 021007

Precision Measurement of the $6S_{1/2}-7P_{1/2}$ Cesium Transition Radial Matrix Element via Simultaneous Absorption Spectroscopy

E. Putney, A. Damitz, G. Toh, D. Elliott

Parity non-conservation in cesium electronic transitions has gathered significant interest over the past several decades, providing opportunities to probe the strength of the weak interaction. Through precise measurement of the strength of classically permitted cesium transitions, such as $6S_{1/2}-7P_{1/2}$ and $6S-7P_{3/2}$, the strength of the classically forbidden parity non-conserving $6S_{1/2}-7S_{1/2}$ transition may be better understood. This measurement aims to refine the known strength of the $6S_{1/2}-7P_{1/2}$ transition through simultaneous measurement of absorption strengths of both the $6S_{1/2}-7P_{1/2}$ and $6S-7P_{3/2}$ transitions. When these measurements are made simultaneously the precise calculation of a radial matrix element, a quantity that describes the absorption strength of a transition, is possible when the other radial matrix element is already precisely known. This methodology eliminates the need for knowledge of other parameters to calculate the unknown radial matrix element, notably the density of the cesium and the length of the cell.

This experiment employs two Littrow configuration external-cavity diode lasers tuned to resonance with the $6S_{1/2}-7P_{1/2}$ and $6S_{1/2}-7P_{3/2}$ transitions, at 459.4 nm and 455.6 nm, respectively. The external cavity of the laser employs a diffraction grating that serves as both a cavity mirror and a monochromator, with a transmitted frequency that changes as a function of angle of incidence between the grating and the beam. These diffraction gratings are attached to mounts that are fine-tunable by piezo-electrics. When a ramped voltage is applied to these piezo-electrics a small, mostly linear scan in transmitted frequency is created through slight changes in the angle of incidence. These scans permit single mode operation, in which the laser emits a very small spread of frequencies, with a typical range of approximately 1-5 GHz. These beams are combined, sent through a heated cesium cell, and are afterwards detected by a photodiode on the other side of the cell. During measurement, one beam passes through the cell while the other is blocked, and an absorption spectrum can be recorded by the photodiode as the laser scans through frequency. Then, before the temperature and density of the cell can drift significantly, the lasers are switched, and a spectrum is recorded for the other beam. This is done in succession several times at each temperature.

Technical complications quickly arise in designing a system to achieve this. The transmitted frequency of these laser diodes is a function of several parameters: the angle of incidence with the diffraction grating, the temperature (related to the external cavity length), and the current driven through the laser diode. Constant control of these parameters for both lasers is paramount to smooth, single mode performance. Because of this, we needed control electronics to be designed and/or calibrated to monitor and stabilize everything. This measurement requires a scan range of approximately 5-10 GHz, the scan range from just the PZT adjustment is not sufficient for a full Doppler-broadened absorption spectrum. A

synchronized and tunable drive-current ramp is required for single mode scans from 5-10 GHz. When the drive current is ramped, stabilization of laser power is also necessary as changes in drive current will change laser power. Each laser utilizes an acousto-optical feedback loop to power stabilize to a given setpoint. Careful temperature stabilization of the cesium cell is also important. A thermo-electric cooler can be employed to stabilize the temperature of the cesium cell cold finger, which is kept around 15K below the temperature of the cell body. The cold finger is the location where cesium condenses, so that no solid cesium builds up on the optical-grade windows of the cell. The cell body is heated by heat rope to some equilibrium temperature and is monitored by a thermocouple. Because the laser is only mostly single mode, it is also important to understand approximately how much power of the cell is in off-resonance modes that won't be absorbed by the cesium. To do so, another cesium test cell is placed in the path and is heated to approximately 400 Kelvin. At this temperature, nearly all laser power on resonance with the transition is absorbed, so that the remaining laser power must be from off-resonance modes. This power is subtracted as an offset constant from the absorption spectra measurements. Finally, because a precise measure of the absorbance is critical to this measurement, saturation of the transition in the beam path cannot be allowed. To avoid this effect, the laser intensity through the cell is about eight thousand times below saturation intensity. Because of this, only approximately 80 nW of laser power transmits through the cell which requires an extremely sensitive, well shielded, low noise photodiode for absorption spectrum measurement.

My summer project involved designing and/or calibrating these systems. Some of these systems had already been built for other projects but were not well suited initially for my own. I considered the needs of the experiment to achieve a measurement to .1% precision, performed the experiment, and wrote data analysis software. We are presently carrying out data analysis to determine the radial matrix element of the cesium $6S_{1/2}$ - $7P_{1/2}$ transition to a very high precision. Preliminary analysis shows consistency with the results of prior literature, but more analysis needs to be completed with some refinements to the experimental procedure to address several possible sources of error.

This work was supported by NSF REU grant PHY-1460899

Majorana Spin Flips in Trapped Antihydrogen

Colin Riggert¹, Miguel Alarcon², Francis Robicheaux³

¹The University of Oklahoma, OK, USA

²Universidad de los Andes, Colombia

³Purdue University, IN, USA

In 2010, the ALPHA collaboration at CERN successfully performed the first magnetic trapping of neutral antihydrogen, trapping 38 atoms for 0.17 s [1]. Shortly thereafter, the collaboration improved their trapping techniques, and in 2011, were able to trap a larger population of atoms for times in excess of 1000 s [2]. These stable trappings offer the opportunity to perform precision spectroscopic measurements of the energy levels of antihydrogen. As CPT theorem holds that antihydrogen and hydrogen should have identical energy level structures, these measurements in turn offer a method of experimentally testing the validity of CPT theorem [1]. However, the magnetic fields involved in trapping the antihydrogen also introduce Zeeman splitting to the antihydrogen energy level structure [3], and the resulting broadening of line widths reduces the value of these measurements for testing CPT theorem. Therefore, to minimize this Zeeman splitting, it becomes desirable to operate the ALPHA trap at low magnetic field strengths. If the field strength is lowered to the extent that points of zero field strength are introduced to the field, adiabatic approximations of the system can break down near these zeros, and atoms in the trap can undergo Majorana spin flips and transition from trapped to anti-trapped spin states, resulting in escape from the trap [4-5]. Through the course of this research, we created models of the ALPHA trap, and numerically solved the Schrodinger equation for the system in order to computationally model these spin flip transitions and the resulting loss characteristics of the trap.

Antihydrogen is a spin-1 particle, with Majorana spin flips occurring among the triplet states of the atom. The resulting three-state problem is computationally sophisticated, so we began by considering a simplified model with a spin-1/2 particle in a linearly varying magnetic field with a central zero. Using the methods developed by Majorana in [6], we generated an analytic value for the cross section, σ , of spin flip transitions around this zero. Using Monte Carlo techniques, we verified the validity of this expression. As the ALPHA trap uses an octupole field for radial confinement, we then considered the combination of a linear field and an octupole field. From this, we found that this combination results in five total zeros in the field, all of the same linear shape as the central zero. After numerically verifying that these five zeroes do not experience any meaningful coherent interference, we then summed their individual analytic cross sections to generate a total analytic cross section for spin-flips in the system.

Using the methods presented in [7], we then generalized these results for the case of a spin-1 particle in the linear field with the octupole turned on. Again, we analytically derived a cross section for the individual zeroes, as well as a total cross section for the system, and were able to numerically verify these cross sections.

Next, we developed a more sophisticated and realistic model of the trap field as a combination of a constant external field, a quadratically-varying field, and the octupole field. While the exact solution for the spin flip cannot be analytically derived as it was previously, we used our existing, proven models to numerically calculate the cross sections through Monte Carlo simulations. With the appropriate field strengths of the component fields in the ALPHA trap, we generated cross sections for various values of the

constant magnetic field in the axial direction of the trap. We also considered the first order linear approximation of each zero in the field, the form of which was calculated with a first order Taylor series. Using our previously found analytic results we then used this approximation to calculate the cross section that would arise if each zero was purely linear in shape.

We found that interesting behavior of the field zeros and their cross sections occurs when the external constant field has a value approximately between $-10 \mu\text{T}$ and $10 \mu\text{T}$. Unfortunately, the ALPHA trap only offers control of this external field in increments of approximately 1 mT. Consequently, this uniquely quadratic behavior is not of meaningful experimental importance, as it lies in a region more than an order of magnitude below the lower limit of control for the ALPHA trap. Further, we found that for values of the field strength greater than 0.1 mT and less than -0.1 mT , the numerically generated cross sections match the analytic cross sections from the first order approximation of each zero to at least four significant figures. These sub-mT bounds are still below the lower limit of control for the ALPHA trap. As a result, any spin-flip loss in the ALPHA trap occurring during actual experimental operation can be described with the previously described analytic solution to the linear case as described in [6] and [7].

The numerical value of the overall cross section for spin-flips in the system varies depending on the exact value of the external field and the velocity of the atom through the trap. Due to the cooling requirements of the trap, the upper limit of velocities in the trap is approximately 70 ms^{-1} , with a population density that varies linearly with energy, and thus with the square root of velocity. With this information, we were able to calculate the lifetime due to spin-flip loss, τ , of atoms with a velocity v_0 as $\tau = \frac{V_{\text{trap}}}{v_0 \sigma}$, where

V_{trap} is the volume of the trap, and σ is the cross section of the spin-flip interaction. We found that even for the highest velocity atoms in the trap, the resulting lifetime of the atoms in a trapped state is still on the order of 1000 s, with slower atoms having much longer lifetimes. These lifetimes are long enough that spectroscopy of the trapped antihydrogen is still possible in low field strength trappings. Therefore, we have concluded that low field strength experiments with the ALPHA trap are feasible. We expect the ALPHA collaboration to conduct experiments in the near future to further investigate these results.

I have grown and learned tremendous amounts because of this REU program experience and am incredibly grateful to Purdue University for this opportunity. I would like to thank my advisor, Dr. Francis Robicheaux, for his constant advice, guidance, and mentorship. I would also like to thank Miguel Alarcon for his constant support as both a colleague and a friend. This work was supported by NSF REU grant PHY-1460899.

[1] G.B. Andersen, et al., ALPHA collaboration *Nature* **468**, 673–676 (2010)

[2] G.B. Andersen, et al., ALPHA collaboration *Nature Physics*, **7** (7), 558-564. (2011)

[3] C.J. Foot *Atomic Physics* (OUP Oxford 2005)

[4] D. M. Brink and C. V. Sukumar, *Phys. Rev. A* **74**, 035401, 11 September 2006

[5] D. M. Brink and C. V. Sukumar, *Phys. Rev. A* **56**(3):2451-2454 · September 1997

[6] E. Majorana, *Il Nuovo Cimento* 1924-1942, **9**(2), pp. 43–50, Feb. 1932

[7] N.A. Sinitsyn, J. Lin, V.Y. Chernyak, *Phys. Rev. A* **95**, 012140, January 2017

Exciton Diffusion Simulations For PDI Molecular Aggregates

Melissa Popeil¹, Tong Zhu², Shibin Deng², Sergei Savikhin², Libai Huang²

¹Binghamton University, NY ²Purdue University, IN

Third generation solar cells can be made of organic materials which would make for exciting new technology that has lower temperature synthesis, is cheap, scalable, and flexible. While organic photovoltaics (OPV) have many desirable properties, their efficiency is lower largely due to a limit in the diffusion length of excitons. The low dielectric constant of organic materials leads to tightly bound electron hole pairs, so called "Frenkel excitons". The Frenkel excitons can only travel about 10 nm, due to the materials low diffusion coefficient, which is far from sufficient for light absorption. Transient absorption microscopy (TAM) is employed to directly visualize Frenkel exciton transport in organic semiconductors with temporal resolution of ~200 fs and diffraction-limited spatial resolution. The objective for my research project was to simulate exciton diffusion for organic materials in order to compare to TAM experimental results.

Exciton diffusion can be modeled using the Forester Resonant Energy Transfer (FRET) which has a transfer rate inversely proportional to r^6 , where r is the distance between the donor and the acceptor. In the simulation, a lattice is constructed and rates for each hopping site are calculated. Increasing the number of lattice sites help to make the simulation more statistical. From there, the shortest time for exciton transfer is found and the site correlated with this time is used as the next hopping site. This runs until the maximum time specified in the code is reached. The TAM experiments collect data that reflect the spatial distribution of exciton population at delayed time points from the initial excitation with a time resolution of ~100 fs. The simulation takes the resolution of experimental data into account. A variable in the code is the hopping time of the exciton. By changing the variable, the simulation can be made to match the experimental results. Trapping of excitons can be incorporated into the code, as well, because low-energy defects sites are expected in molecular aggregates. This code will be used to model the exciton diffusion of perylene diimide (PDI) molecular aggregates and the ultimate goal is to provide insight for better performing OPV.

Acknowledgements:

I am grateful for the opportunity to be a part of the REU program at Purdue. I would like to thank Prof. Libai Huang, Prof. Sergei Savikhin, Dr. Tong Zhu, and Dr. Shibin Deng for their guidance throughout this experience. I would also like to thank NSF REU grant PHY-1460899 for supporting my work.

Computational Studies of Energy Transfer within FMO Mutant Structures

Scott McKinley¹, Yongbin Kim², Lyudmila Slipchenko²

¹University of Arizona, Department of Physics, Tucson, AZ 85721

²Purdue University, Department of Chemistry, West Lafayette, IN 47907

Over billions of years, nature has perfected the photosynthetic process. In bacteria, for example, light energy is transferred to the photosynthetic reaction center by 8 bacteriochlorophylls within the Fenna-Mathews-Olson (FMO) complex with nearly 100% efficiency. Understanding the details of this complex will provide new insights into how artificial light-harvesting devices can be constructed. This work focuses on computationally modeling 8 FMO mutant structures for which spectroscopic data are available. We produce theoretical absorbance spectra and compare them to the experimental results. The ability to reproduce the results from first principles would be a major step toward understanding energy transfer within the FMO complex.

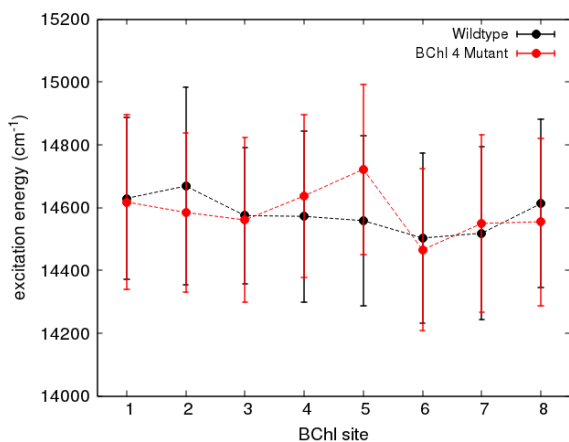


Figure 1: First excitation energies of all 8 bacteriochlorophyll sites in mutant 4 and in the wildtype structure, averaged over 100 trajectory snapshots.

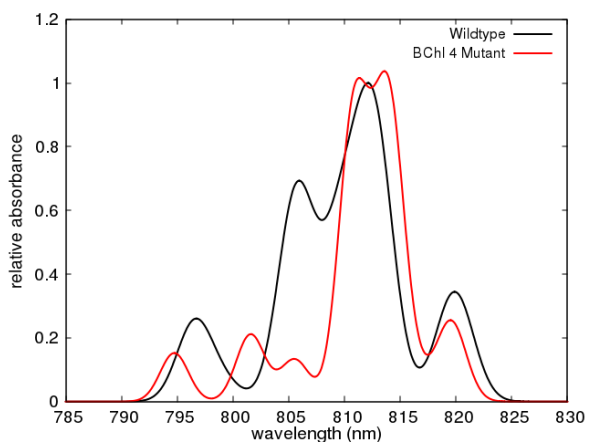


Figure 2: Calculated absorbance spectrum for mutant 4 and the wildtype structure.

The calculation of spectra first requires the motion of each structure to be simulated. An FMO mutant is constructed by taking the natural, or wildtype, form of the complex and changing a single amino acid in the protein environment near one bacteriochlorophyll. We introduce each mutant into a water environment and perform molecular dynamics simulations using GROMACS software. After the structure equilibrates in its environment, we take 100 snapshots of its trajectory for further analysis. Next, we use GAMESS software to perform quantum mechanical calculations on each bacteriochlorophyll in each snapshot. The calculations yield first excitation energies, shown in Figure 1 for the structure with the mutation near the 4th bacteriochlorophyll, and transition dipole moments. Dipole-dipole interaction energies give the bacteriochlorophyll couplings, which are critical for efficient energy transfer. We determine the absorbance spectra from the site energies and coupling values (Figure 2). Current results agree loosely with experimental results, but additional improvements to both the molecular dynamics model and the quantum mechanics calculation method will need to be implemented.

I would like to thank Lyudmila Slipchenko and Yongbin Kim for their guidance during this outstanding experience at the Purdue Physics REU. This work was supported by NSF REU grant PHY-1460899.

Simulating the Cooling and Trapping of Cesium Atoms onto a Nanophotonic Waveguide

Kevin Knox-SUNY Oneonta, Brian Fields-Purdue University, Tzu-Han-Chang-Purdue University, Chen-Lung Hung-Purdue University

Purdue University, IN

Quantum interactions happen in two extremes: small length scales and cold temperatures. Dr. Chen-Lung Hung's research group is designing an apparatus which will allow us to investigate quantum systems of the extreme cold. This apparatus will trap, cool and isolate Cesium atoms and will allow us to observe their long-range quantum interactions mediated by a photon.

My objective was to modify and build upon a Monte Carlo simulation in MATLAB which tracks the behavior of the Cesium atoms when entering a random face of the optical potential trap while also being laser cooled via the molasses technique. This was simulating the method which my research group is planning to lower individual, cold Cesium atoms onto a nanophotonic waveguide to observe their quantum interactions mediated by a photon. The goal of the simulation was to replicate the conditions of the experiment and vary parameters, like temperature, to see which conditions optimize the percentage of atoms that remain eligible to place onto the membrane. The program loads an atom at a random boundary of the trap with a speed sampled from a Maxwell-Boltzmann distribution corresponding to the desired starting temperature. The speed is assigned a random direction and is corrected to point towards the trap. The position of the atom is tracked on an infinitesimal grid, while the potential is resolved with grid spacing of 25 micrometers. The force on the atom from the potential is averaged from the nearest points on its grid. The atom is subject to scattering forces from the laser cooling, which takes advantage of Cesium's D-2 transition, as well as gravity. The scattering rate varies with the velocity of the atom through its level of detuning from the laser, which takes advantage of the Doppler Effect.

The potential begins as a large "back-tweezer", which consists of a few large, attractive lobes. Throughout the simulation time, it transitions into a finer potential with several lobes in xy-planes of increasing height. The atom's position is traced through small time steps, and its final position is saved at the end of the simulation time. This process is then repeated for 250,000 atoms, and we calculate fraction of atoms remaining in the trap and which of those were in the bottom lobe of the trap. We found that about 0.1% of atoms which entered the trap remained in the trap after the simulation time of 200 microseconds, with about 80% of those trapped in the bottom lobe. The simulation was then repeated for increasing temperatures and their outputs were plotted against temperature. The program can be run through Purdue's Halstead cluster, which allows for faster and more powerful calculations. The code can be modified to show changes in output against any varying parameter or starting condition.

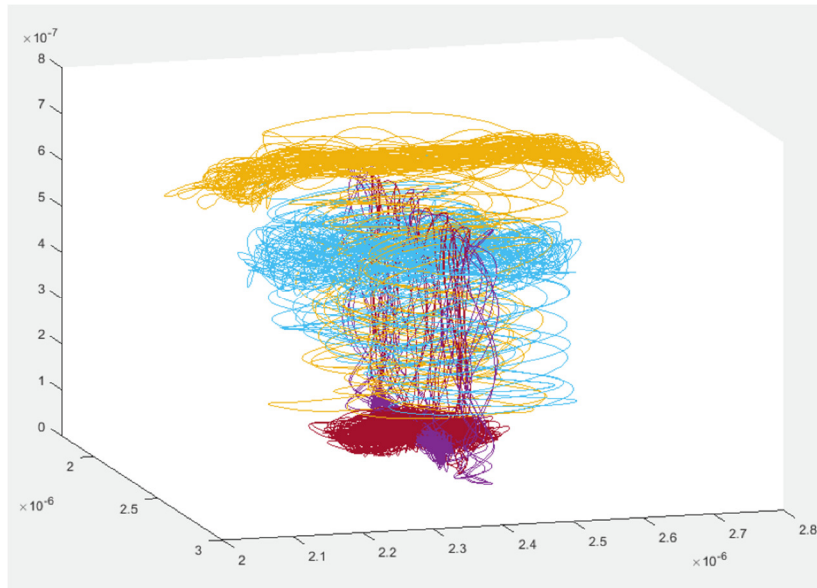


Figure 1

The trajectories of four atoms which remained trapped at the end of the simulation. Created in MATLAB

I continued to build off this simulation and created a variation of this simulation which will track and save the trajectories of the atoms which remained trapped at the end of the simulation time [Figure 1]. This was useful to visibly see the dynamics of atom's movement within the trap and determine exactly where the atoms should begin to produce the best trapping rates. One last variation of the code was made, which ramped on the back-tweezer and top-tweezer simultaneously.

I would like to thank and acknowledge my advisor, Dr. Chen-Lung Hung and the rest of his research group for their guidance and support. This work was funded and supported by NSF REU grant PHY-1460899.

Using Magnetic Tweezers to Examine Protein Mechanics

Caitlin Gish^{1,2}, Jian-yu Chen², Ken Ritchie²

¹University of South Florida, FL; ²Purdue University, IN

In the work we have done, we have used magnetic tweezers to create a magnetic field gradient that allows us to control the amount of force being applied to a magnetic bead that has been attached to the end of a protein L chain that has been engineered to have a chain of eight proteins. Using eight proteins makes it easy to identify the protein when performing experiments. As can be seen in Figure 1A, when the protein L is put under a sufficiently high force the eight proteins will unfold sequentially in a recognizable stair step. Once the protein has been identified, then a force that is large enough to unfold some of the proteins but not all eight is applied and the protein can be observed to jump back and forth between different levels, demonstrating the protein both unfolding and refolding under a constant force (Figure 1B). The goal of this project is to investigate this jumping back and forth in more detail to see what this shows about the free energy of a protein and the probability of a protein chain under constant force having any number of folded or unfolded proteins. Utilizing this information, the next step after this would be to investigate the thermodynamic properties of proteins.

While it is known that chains of amino acids form proteins, little is known about how these chains determine the three-dimensional structure of a given protein. Little is also known about the energy of a protein in its folded or unfolded state. Because of the importance of proteins at both the cellular and organism level, learning more about the way proteins fold and unfold will open the doors for further understanding of many concepts and processes. An example of one of these processes is the fact that a protein must fold and unfold to enter a cell through the cell membrane. Additionally, some diseases are the result of proteins unfolding or misfolding. The research we are doing could be used to understand better why and how these types of diseases occur.

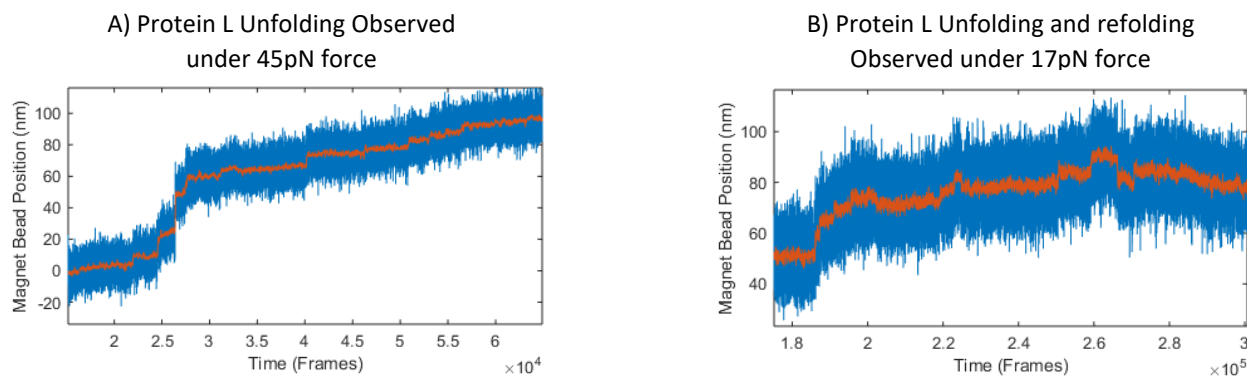


Figure 1

I would like to thank all the Purdue Faculty and Staff who have made this opportunity possible. Especially Ken Ritchie and Jian-yu Chen who I have had the honor to work with on this project.

**This work was supported by NSF REU grant PHY-1460899

Single Electron Backgrounds in Liquid Xenon TPCs

Leesa Brown, Abigail Kopec, Rafael Lang
Purdue University, West Lafayette, IN

Dark matter composes roughly 85% of all matter in the Universe. So far, only the gravitational effects of dark matter have been observed. Dark matter exists within galaxies and in halos surrounding the galaxy. This has given lower limits on the mass of a dark matter particle and an upper limit on its kinetic energy. A leading candidate for a dark matter particle is a weakly interacting massive particle (WIMP). Located at Laboratori Nazionali del Gran Sasso under a mountain in Italy, XENON1T is currently searching for WIMPs with masses between GeV/c^2 and TeV/c^2 . It holds 3.2 t of pure liquid xenon with 2 t used as target volume and a 1.3 t fiducial volume. The WIMP expected to scatter with xenon nucleus or electrons bound to the xenon atom. The recoil produces photons (S1 signal) and due to the electric field, a few outer electrons from the xenon will drift free. These electrons will drift to the top of the liquid xenon and will scintillate in the gaseous xenon (S2 signal). The S1 and S2 signals are detected by the 248 PMTs in the time projection chamber (TPC). Electron trains are a major background in liquid xenon dark matter experiments. These are S2 signals that aren't correlated with a S1 and occur on much longer time scale than is possible for normal events (See Figure 1). The background is possibly caused by electrons without enough initial energy to be extracted to gas because of a potential barrier at the liquid-gas interface. At some later time, these thermalized electrons will all tunnel through into the gas and produce the electron train signal.

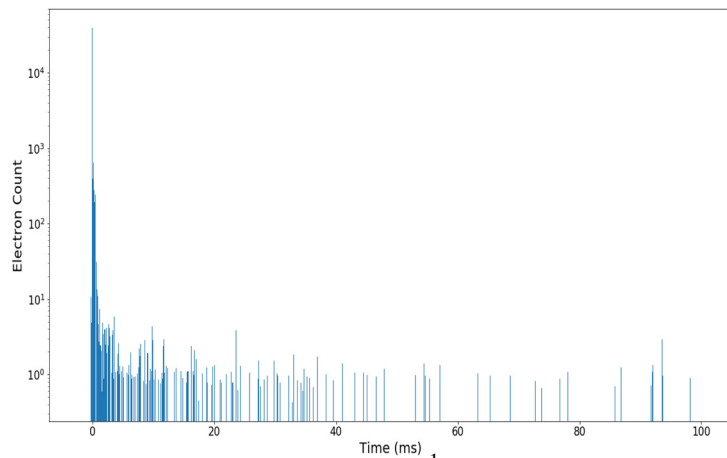


Figure 1¹

My research contributed to the goal of mitigating the single electron background through a possible hardware solution. As the barrier between the liquid and gas interface has a potential of 0.34 eV^[2], if a photon with more energy were to scatter with the electron, it should give the trapped electron enough energy to overcome the barrier. This will be tested with the ASTERiX detector located at Purdue. ASTERiX is similar to XENON1T, but its TPC can hold 6-7 kg of liquid xenon, and has only one array of PMTs. Currently, there is an IR LED and an IR photodiode inside ASTERiX. The LED has a peak wavelength of 1650 nm, so photons from the emitter will have energies of 0.75 eV. The photodiode is used to determine if the LED is on. An external circuit, which I built, amplifies the signal from the photodiode, and is read by an oscilloscope. Currently, the signal from the photodiode is very noisy, and the signal was lost when the detector was filled with liquid xenon. It was hypothesized that the temperature of the liquid xenon was too cold for the IR LED. Under vacuum, the signal from the photodiode had amplitude of about 270 mV. When we turned off the vacuum pump and starting to fill with xenon, the amplitude decreased to 140 mV. After further filling, the amplitude was down to 70

mV, before disappearing entirely. I tested the IR LED and photodiode in liquid nitrogen. I tested the IR LED and photodiode in a dewar partially filled with liquid nitrogen such that a temperature gradient formed above the liquid level. I lost the signal at -120 °C. This would point to the photodiode or LED in the detector failing due to cold temperatures, however the detector was kept above the triple point of xenon -111 °C. It is unclear why the signal cut out.

In addition to my work with the photodiode, I collected mass spectra with a residual gas analyzer from the gas vacuumed from the detector. From this, I determined that recirculating gaseous xenon through ASTERiX was the most efficient process to remove hydrocarbons from the detector. Due to the copper wires inside the detector, recirculation increased the copper peaks in the mass spectrum. To mitigate the copper, I recommend heating the detector while running the vacuum pumps for a few days.

This work was supported by NSF REU grant PHY-1460899 and NSF grant 1719271.

¹Amanda Depoian

²<https://arxiv.org/abs/1702.04805>

Using Chemically-Induced Micro-Seismicity to Image Transport in Fractures

William Braverman¹ and Laura J. Pyrak-Nolte²

¹The College of New Jersey, NJ

²Purdue University, IN

This is proprietary work and will be made public elsewhere

I am grateful for the opportunity to be a part of the REU program at Purdue. I would like to thank Dr. Laura J. Pyrak-Nolte as well as her grad students for their guidance throughout this experience. I would also like to thank NSF REU grant PHY-1460899 for supporting my work. This work is supported by the U.S. Department of Energy, Office of Science, Office of Basic Energy Sciences, Geosciences Research Program under Award Number (DE-FG02-09ER16022)